Electromechanical Energy Conversion Systems (EECS)
Niroo Research Institute (NRI)
Vol. 3, No. 1, Autumn 2024, 9-17
DOI: 10.30503/eecs.2024.458400.1052
Original Article

Axial Flux Permanent Magnet-Hysteresis Motor with Single Disc Rotor: Torque Comparison of Different Structure

Hashem Yousefi Javid[1*], Aydin Yousefi Javid[2]

Abstract

Axial flux hysteresis motor has the advantages of hysteresis motors such as self-starting, constant torque, smooth operation, no oscillation and noise, and also the advantages of axial flux structure such as high torque in the same dimension, adjustable air gap and multi-stack. However, due to the low energy level of the hysteresis material, this type of motor has a low torque level. In this paper, to improve torque, various proposed structures have been implemented on the disc of axial flux hysteresis motor and subsequently compared. According to the results, the motor with the highest torque in the same dimensions and simple structure is preferred. To model the hysteresis motor, the elliptical method has been used considering its speed and accuracy. Then, the analytical equations governing the proposed structures are presented. Finally, the torque calculations of different structures have been performed and analyzed using the finite element analytical method. The results show that in some of the proposed structures, the torque has improved significantly compared to the original hysteresis motor.

Keywords: Axial flux motor, Finite element analysis, Hysteresis motor, Permanent magnet motor, Torque calculation.

Received Date: 2024-05-19 ; Revised Date: 2024-06-20 ; Accepted Date: 2024-06-24

1. INTRODUCTION

Hysteresis motor has the advantages of a constant torque, simple structure, high-speed operation, high temperature resistance, low noise, low starting current and self-starting capability. However, low torque density, low efficiency and low power factor are referred to as its disadvantages. Radial flux permanent magnet hysteresis synchronous (PMHS) motor has the advantages and performance characteristics of both permanent magnet and hysteresis motors; it benefits from the self-starting feature of hysteresis material during starting and steady state, as well as from the high energy level and proper efficiency of the permanent magnet [1-2]. Radial flux PMHS motor is used for high-speed applications, submersible pumps and electric vehicles .In these motors, a hysteresis ring with magnet fragments is used in the cylindrical structure of the motor's rotor. Occasionally, instead of the magnet fragments, a magnet ring is used [3-5]. In order to increase the torque of the radial flux hysteresis motor, by creating gaps on its rotor, reluctance hysteresis motor has been presented, which later became a radial flux permanent magnet hysteresis motor by placing a magnet in those gaps [6-7].

Considering the problems of hysteresis loop modeling, accuracy in the modeling and analysis of this type of motors is important; therefore, it has been discussed in various references [8-13].

Conventionally, the structure of a synchronous motor is radial flux, but due to their advantageous features, axial flux motors, have been noted recently. Seemingly, axial flux motors are more compressed compared to radial flux motors, i.e., they have a higher density and power. The air gap in these motors is easily adjusted. Axial flux motors can also be built modular. In another word, using multi-stack structure can help acquire the desirable power and torque [14-15]. One of the famous axial flux motors is the axial flux permanent magnet synchronous motor. This type of motor has proper torque in steady state but lacks starting torque which is provided by drive system or rotor's induction structure [16].

Axial flux hysteresis motors, despite having the advantages of both the hysteresis motor and those of the axial flux structure, have lower torque and efficiency. To tackle this problem, the following hybrid structures are proposed:

a) A two-disc axial flux PMHS structure has been suggested. In this topology, one disc is hysteresis and the other one is PM. The results show that the steady state of the motor has improved but the

1 Department of electrical engineering, Iran university of Science and Technology
2 Department of electrical engneering, Islamic Azad University South Tehran Branch
**Corresponding author, hashem_y@cmps2.iust.ac.ir*

starting state, considering the magnet brake torque needs more investigation [17-18].

b) Hybrid hysteresis motor with integrated radial and axial flux [19-20]. According to the results, the torque has increased considerably, but the rotor and stator structures have become complicated.

Furthermore, the axial flux reluctance hysteresis motor has been examined to improve the torque characteristics of the hysteresis motor. In the mentioned study, the rotor volume has increased significantly to create a reluctance gap; therefore, the reluctance torque has not been compared under conditions of similar dimensions [30].

It should be noted that so far, studies lack a structure that combines magnet and hysteresis material on a disc in axial flux motors. The purpose of this paper is to investigate different combinations of hysteresis disc motor using the PM to provide a new hybrid motor topology that has the advantages of hysteresis and magnet motors as well as those of the axial flux structure with the proper torque in the steady and starting modes, and a simple motor structure.

Considering the different energy level of the hysteresis material and the magnet, the way to combine the two types of materials, their figures and volumes is important and should be taken into account. Furthermore, how to achieve the desired structure with the proper torque is also very important. Thus, in this paper, the simulation of different motor structures is done by accurate modeling of hysteresis loop and finite element analysis (FEA) method.

2. MODELING AND EQUATION OF AFPMHM

Generally, the modeling techniques to describe the hysteresis phenomenon are classified into two groups: physical and phenomenological modeling. In physical modeling, the main processes that describe magnetizing are simulated. In phenomenological modeling, the macroscopic behavior of the material is described mathematically creating curves. The latter model is more optimal in terms of calculation compared to the physical modeling, but presents no physical view of the ongoing processes.

Mathematical modeling of the hysteresis phenomenon is divided into two groups: scalar and vectorial. In the scalar model, it is assumed that in every part of the material, the direction of the vectors of magnetic field intensity H(t), magnetic flux density B(t) and magnetization M(t) are fixed over time. The direction of the vector, in some phenomena needs to be changed; therefore, vectorial modeling, which is highly complicated, is required. Scalar models are subdivided into two models: static and dynamic.

It is hypothesized that in static scalar models the amount of magnetization and magnetic flux density depend just on the amount of magnetic field intensity at every moment and the amounts of previous extremums. In other words, the amount of magnetization and magnetic flux density are independent of magnetic field intensity variation speed. The most common static scalar hysteresis models include: Hodgdon's model, Jiles Atherton model and classical Preisach model [21-25],[29]. In the following, approximate models of hysteresis loop modeling are examined.

2.1. Modeling hysteresis loop by elliptical model

In the usual methods for designing and investigating the behavior of hysteresis machines, the accurate modeling of the hysteresis characteristic is usually very difficult; Therefore, in most cases, the approximation of the hysteresis characteristics is used. Two types of common and widely used approximation for hysteresis characteristics are: approximation using ellipses and approximation using parallelograms [26-28]. In the hysteresis motor analysis process, the complex permeability is used to model the hysteresis loop with the elliptical approximation method. Fig. 1 shows the elliptical model of the hysteresis loop. There is a difference in the alpha angle between the maximum flux density and the maximum field intensity. In equations one and two, the magnetic flux density and the intensity of the magnetic field are presented respectively.

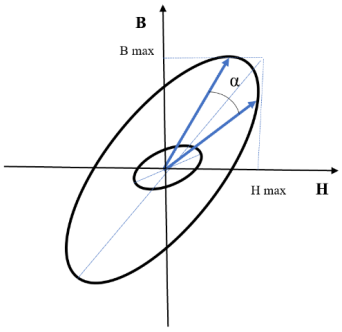

Fig. 1. Elliptical model of a hysteresis loop

$$B = B_m \cos(\omega t - \varphi - \varphi_0) \quad (1)$$

$$H = (\frac{B_m}{\mu}) \cos(\omega t - \varphi - \varphi_0 + \alpha) \quad (2)$$

Where B_m is the maximum flux density of the rotor material, μ is the permeability of the elliptical hysteresis loop, ω is the synchronous angular frequency, φ ($\varphi = p\theta_r$, θ_r is the mechanical

angle of the rotor and p is the number of pole pairs) is the electrical angle coordinate in the stator frame, φ_0 is the phase shift and α is the hysteresis lag angle between B and H. α angle is calculated from equation (3).

$$\alpha = \arcsin \frac{H_c}{H_m} \tag{3}$$

To implement the approximate elliptical model, the complex permeability parameters are calculated according to the equation (5). To calculate the complex permeability parameters, first, the permeability size is calculated according to the equation (4).

$$|\mu_r| = \frac{B_m}{\mu_{r0} H_m} \tag{4}$$

$$\mu = \mu' - j\mu'' = |\mu_r|(\cos\alpha - j\sin\alpha) \tag{5}$$

In this paper, after calculating the parameters of μ' and μ'' using the actual measured magnetic characteristics, μ' and μ'' are applied in Flux 3D software, and elliptical model in the steady state mode is used for FEA of motors.

The magnetic characteristics of the hysteresis material measured by B-H meter are presented in Table 1 and the calculated parameters including μ' and μ'' are 264 and -70, respectively. Fig. 2(a), Fig. 2(b) shows B-H curve of hysteresis material and stator material.

TABLE 1. The magnetic characteristics of the hysteresis material measured by B-H meter

Description	values
Coercive field intensity (Hc)	1300 A/m
Maximum field intensity (Hm)	5000 A/m
Residual flux density (Br)	1.3 T
Maximum flux density (Bm)	1.69 T

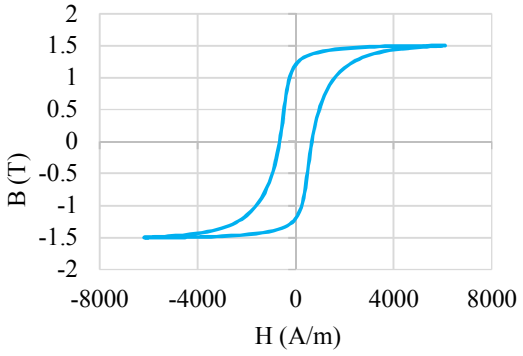

(a)

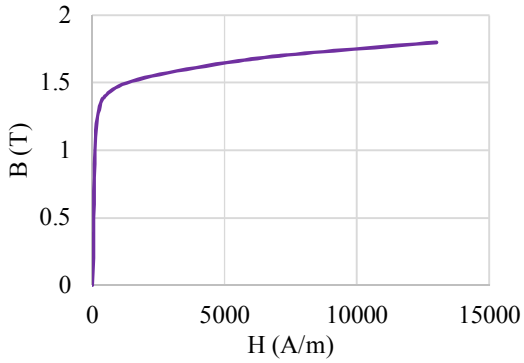

(b)

Fig. 2. B-H curve (a) hysteresis material (b) stator material

2.2. Analytical equations

The equations related to hysteresis torque fragment of the axial flux permanent magnet hysteresis motor (AFPMHM) are as follows:

$$T_{HM} = \frac{p}{4\pi} E_h . V_{HM} \tag{6}$$

Where V_{HM}, p and E_h are volume, the number of poles and hysteresis material energy, respectively. E_h can be calculated from equation (7).

$$E_h = \pi B_{mHM} H_{mHM} \sin\alpha \tag{7}$$

Where B_{mHM} and H_{mHM} are the data of table 1 and $\sin\alpha$ is calculated using equation (3). The volume of the hysteresis disc of the AFPMHM motor is calculated by subtracting the volume of the magnet ring from the hysteresis disc according to equation (8).

$$V_{HM} = \left(\frac{\pi D_{oHM}^2 (1-\lambda_{HM}{}^2) t_h}{4} - \frac{\pi D_{oPM}^2 (1-\lambda_{PM}^2) t_m}{4}\right) \tag{8}$$

Where λ_{HM} and λ_{PM} are the ratio of the hysteresis disc inner diameter to its outer diameter, the ratio of the permanent magnet disc inner diameter to its outer diameter, respectively. Hysteresis magnetic flux density of the air gap and HM current is calculated using equation (9) and (10) [37].

$$B_{gHM} = \frac{2B_{mHM} t_h}{\frac{2\pi R_{avg}}{p}} \tag{9}$$

Where R_{avg}, g, μ_0, μ, m, N_1 and a are the average radius of hysteresis disc, airgap length, magnetic permeability of air, permeability of hysteresis, phase number, number of rounds of each phase and parallel path respectively.

$$I_s = \frac{B_{mHM}\sqrt{(\frac{gpt_h}{2\mu_0 R_{avg}})^2 + (\frac{2R_{avg}}{p\mu})^2 + \frac{2gt_h}{\mu_0\mu}\cos\alpha}}{\frac{mN_1\sqrt{2}}{2pa}} \quad (10)$$

The equations related to PM torque fragment of the AFPMHM motor are as follows [13]:

$$T_{PM} = \frac{\pi}{8} B_{avgPM} A_{in} K_d \lambda_{PM} (1-\lambda_{PM}^2) D_{oPM}^3 \quad (11)$$

Where B_{avgPM} is average air-gap flux density over a pole, A_{in} is electrical loading at the inner radius. Also, K_d is distribution factor. B_{avgPM} is considered equal to B_{gHM} according to equation (11) and A_{in} is calculated from equation (12).

$$A_{in} = \frac{m_1\sqrt{2}N_1 I_s}{\pi r_{in}} \quad (12)$$

The torque value of AFPMHM can be calculated from equation (13).

$$T_{PMHM} = T_{HM} + T_{PM} \quad (13)$$

By inserting the equation (6) and (11) in the equation (13), the final equation of the torque of the AFPMHM is presented in the equation (14).

$$T_{PMHM} = \frac{p}{4\pi} E \left(\frac{\pi D_{oHM}^2 (1-\lambda_{HM}{}^2) t_h}{4} - \frac{\pi D_{oPM}^2 (1-\lambda_{PM}^2) t_m}{4}\right) + \frac{\pi}{8} B_{avgPM} A_{in} K_d \lambda_{PM} (1-\lambda_{PM}^2) D_{oPM}^3 \quad (14)$$

The equations related to the axial flux reluctance hysteresis motor (AFRHM) are as follows [6]:

$$T_{RHM} = T_{HM} + T_{RM} \quad (15)$$

$$T_{RHM} = \frac{\omega}{2}(\psi_d I_q - \psi_q I_d) = \frac{mP}{2\omega_s}\frac{V^2(x_d - x_q)}{(x_d x_q - R_d R_q)^2}\left\{x_q R_d \cos^2\delta - x_d R_q . \sin^2\delta + \frac{1}{2}(x_d x_q - R_d R_q)\sin 2\delta\right\} \quad (16)$$

Where ω_s, x_d, x_q, V, δ, R_d and R_q are the synchronous speed, d- and q-axes reactance, applied phase voltage, torque angle, d- and q-axes combined resistances respectively.

$$R_d = R_s + R_{h_d} \quad (17)$$

$$R_q = R_s + R_{h_q} \quad (18)$$

Where R_{h_d} and R_{h_q} are the d- and q-axes hysteresis resistances of the ring, respectively.

$$R_{h_d} = \frac{mE_g^2}{4B_r H_c V_d f} \quad (19)$$

$$R_{h_q} = \frac{mE_g^2}{4B_r H_c V_q f} \quad (20)$$

Where E_g, B_r, f, $V_{d'}$ and $V_{q'}$ are the phase voltage at air gap, residual flux density in the hysteresis material, frequency, volume of the hysteresis ring in d axis and volume of the hysteresis ring in q axis respectively.

3. ANALYSIS OF VARIOUS STRUCTURE

3.1. Introducing different types of proposed structures

The reference motor of the current paper is an axial flux hysteresis motor according to [19] and [28]. In what follows, axial flux hysteresis motor is called hysteresis motor (HM). According to the Fig. 3 in this motor, the magnetic flux is axial in the air gap and the magnetic flux in the hysteresis disc of the rotor is peripheral. Table 2 presents the features of the HM.

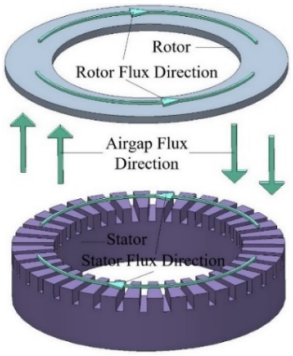

Fig. 3. The structure and flux line of HM

Despite the advantages of hysteresis motors, including optimal starting torque, the reference motor has a low maximum torque due to the low energy level of the hysteresis material. Therefore, to increase the torque of the motor, adding the radial flux structure to the axial flux structure has been suggested in [16].

TABLE. 2. Characteristics of axial flux hysteresis motor

Description	values
Rotor outer radius	57 mm
Rotor inner radius	38 mm
Disc thickness	3 mm
Coercive field intensity	1300 A/m
Residual flux density	1.3 T
Stator outer radius	55 mm
Stator inner radius	38 mm
Core height	23 mm
Slot opening	3 mm
Number of slots	36
Air-gap length	2 mm
Number of poles	2
Number of phases	3
Turns per pole per phase	180 Turn
Fundamental supply frequency	50 Hz
Relative permeability	1000
nominal voltage	15 v
nominal speed	3000 rpm

In the present study, the attempt is to use simple structures to increase the torque of the motor. The proposed structures are all mounted on an axial flux motor disc.

The purpose of this paper is to achieve a structure that increases the steady state torque of the axial flux hysteresis motor in the similar dimensions. This is done by adding reluctance, magnet fragment or magnet ring to the hysteresis disc; hence, the proposed motor is expected to have a proper torque in both starting and steady modes.

The suggested structures of Fig. 4 to Fig. 7 were inspired by radial flux permanent magnet hysteresis motors [1-5], radial and axial flux permanent magnet motors [11], [12], [32-36] and axial flux hysteresis and axial flux reluctance hysteresis motors [19], [30-31].

In Fig. 3, the HM which was the reference motor is presented. Fig. 4 to Fig. 7 present the proposed structures of the motor rotor. Fig. 4(a) is reluctance hysteresis motor 1 (RHM1). In this motor, the attempt is made to add the reluctance torque to the hysteresis torque by creating a reluctance on the hysteresis disc.

In Fig. 4(b), by adding magnet fragments and charging them in line with the hysteresis disc flux, the torque is expected to increase. The above-mentioned motor is called permanent magnet hysteresis motor1 (PMHM1).

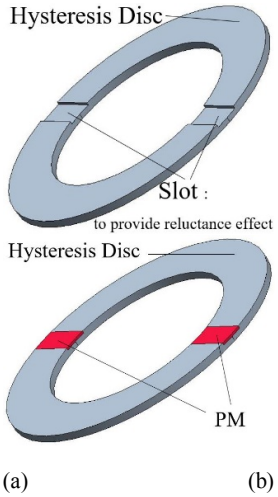

Fig. 4. The rotor structure of proposed motors, (a) RHM1, (b) PMHM1.

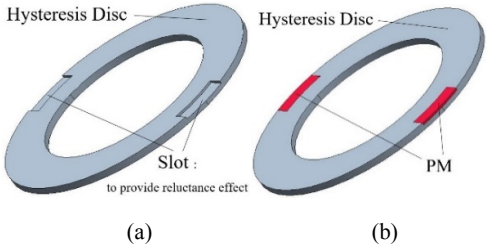

Fig. 5. The rotor structure of proposed motors, (a) RHM2, (b) PMHM2.

In Fig. 5(a), the reluctance is created in a part of the cross-section and towards the outer diameter, and in Fig. 5(b), the magnet is embedded in the disc and is charged in the direction of the disc flux. The motors of Fig. 5(a) and Fig. 5(b) are called reluctance hysteresis motor2 (RHM2) and permanent magnet hysteresis motor2 (PMHM2) respectively.

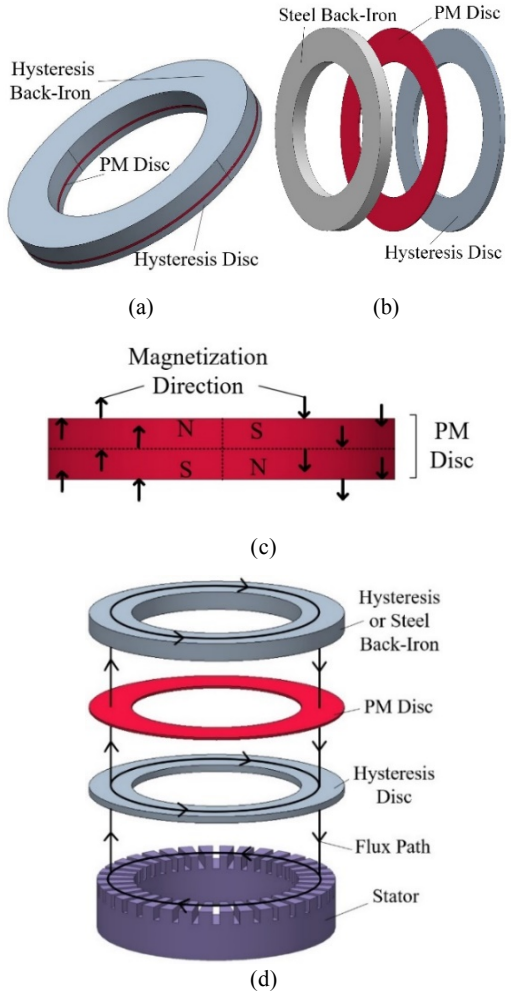

Fig. 6. The rotor structure of proposed motors, (a) PMHM-HB, (b) PMHM-SB, (c) magnetization direction of PM, (d) Magnetic flux path of motors PMHM-HB and PMHM-SB.

In Fig. 6(a) the rotor shows three discs, the lower one is the hysteresis, the middle disc is the magnet, and the upper disc is the hysteresis back iron. The name of the motor is permanent magnet hysteresis motor with hysteresis back iron (PMHM-HB). Fig. 6(b) is similar to Fig. 6(a) with the difference that steel back iron is used instead of hysteresis back iron. The name of the motor of Fig. 6(b) is permanent magnet hysteresis motor with steel back iron (PMHM-SB). PMHM-HB, PMHM-SB are more voluminous than the other eight rotors due to the need for a thicker back iron, but the other eight proposed rotors have the similar dimensions. Fig. 6(c) shows the magnetic direction of the PM disc where the flux path is axial. In Figure 6(d), the magnetic flux path of both PMHM-HB and PMHM-SB motors is shown. The flux resulting from the hysteresis disk enters one pole (S_N) of the magnet vertically and leaves it vertically and enters the back iron then returns from the second pole in the opposite direction (N_S).

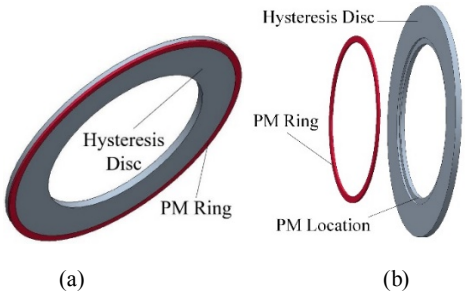

Fig. 7. The rotor structure of proposed motors, (a) AFOPMHM, (b) AFIPMHM.

In Fig. 7(a) the axial flux outer permanent magnet hysteresis motor (AFOPMHM) is presented. In this motor, the magnet ring is placed in the outer diameter of the hysteresis disc. The magnet ring is axially charged. The magnetic flux moves axially from the air gap and enters the hysteresis disc and magnet ring parallelly. Moreover, a hysteresis back iron, which is made integral with the main hysteresis disc, is used. Fig. 7(b) is similar to Fig. 7(a) with the difference that the magnet ring is inside the diameter of the hysteresis disc. This motor is referred to as axial flux internal permanent magnet hysteresis motor (AFIPMHM).

3.2. FEA of different motor structures

In order to achieve the proposed motor structure, Fig. 4 to Fig. 7 structures is analyzed by finite element. Due to the appropriate speed of modeling by elliptic method, in order to compare different motor structures, finite element analysis has been done by
elliptical method. First, the HM with the specifications of the Table 2 is analyzed by the elliptical modeling method.

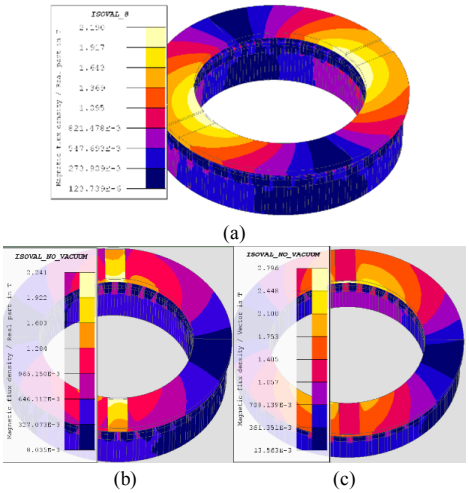

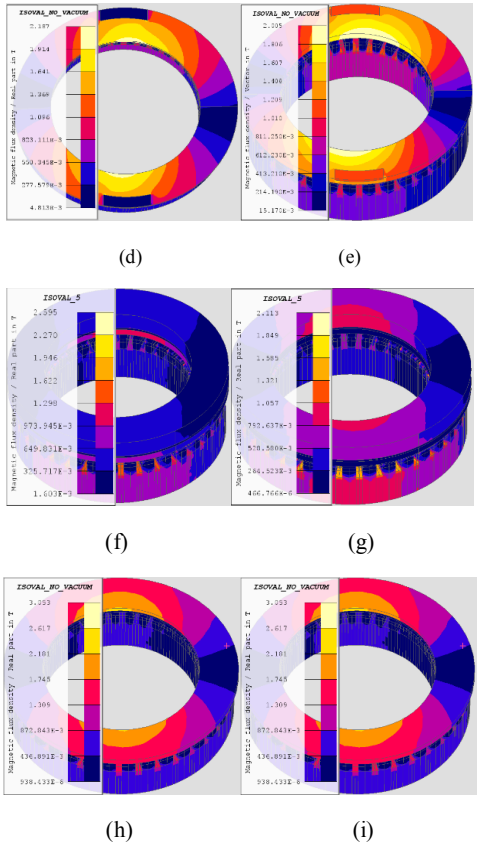

(d) (e)

(f) (g)

(h) (i)

Fig. 8. Flux density of different motor structures. (a) HM, (b) RHM1, (c) PMHM1, (d) RHM2, (e) PMHM2, (f) PMHM-HB, (g) PMHM-SB, (h) AFOPMHM, (i) AFIPMHM.

To use the elliptical model, the real data of the B-H curve for the semi-hard material has been measured (Table 1.). Then, using the data of the B-H curve, μ' , μ'' are calculated according to the equation (5) and used as an input to the Flux finite element software. In the meshing of the proposed motor, all kinds of meshing shapes and their different sizes have been investigated. Finally, the simulation has been done with desirable accuracy**.**

Figure 8 shows the magnetic flux density of different motor structures. The goal is to obtain the maximum torque for each structure. To achieve this, the simulation is performed up to the maximum flux density of the hysteresis disc, which is up to 2.2T. In order to reach the maximum flux density and finally the maximum torque, the simulation is in the range of 20v. Though, it is done up to 25 volts for different motor structures.

In Fig. 9 the torque results related to the hysteresis section and the permanent magnet different motor structures are presented. The analysis of the results of Fig. 8 and Fig. 9 is as follows.

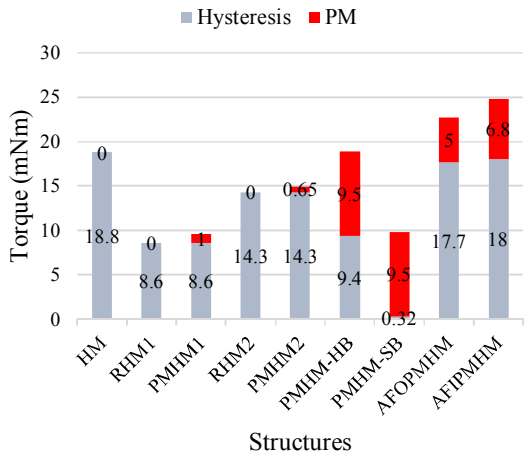

Fig. 9. The torque of different motor structures

The HM torque includes only the hysteresis torque. By creating a reluctance gap in RHM1, it is expected that the reluctance torque will be added to the hysteresis, but the torque decreases. To justify this, it can be said that it is due to the reduction of the cross-sectional area of the hysteresis disc flux at the gap. According to Fig. 8(b) this place goes to saturation faster; thus, less torque is produced. For the PMHM1 motor, despite the addition of the magnet fragment, the produced torque is still lower than HM. In RHM2 and PMHM2 motors, the cross-sectional area of the flux is reduced, but compared to RHM1 and PMHM1, the cross-sectional area is larger, so more torque is produced. In PMHM-HB, one part of the torque is provided by the permanent magnet disc and the other part of the hysteresis disc. In PMHM-SB, due to the use of steel back iron and the low magnetic reluctance of steel compared to the hysteresis material, all the magnetic flux passes through the permanent magnet disc and steel back iron and not through the hysteresis disc. It can be concluded that only the magnet disc's torque is produced. PMHM-HB and PMHM-SB, despite having a larger rotor volume compared to other structures, do not produce a lot of total torque due to the point saturation of the stator. In AFOPMHM, a magnet ring is placed in the outer diameter of the hysteresis disc with a hysteresis back iron so that the hysteresis disc and the hysteresis back iron are integrated. In this motor, the hysteresis torque is almost the same as that of the HM, and the torque of the magnet ring is added to it. AFIPMHM is similar AFOPMHM With the difference that the magnet ring is placed in the inner diameter of the hysteresis disc and they both have almost the same torque, but regarding the problems related to the motor construction, AFIPMHM is preferable due to the smaller diameter

of the magnet. Comparing the maximum torque and simplicity of different structures, AFIPMHM is introduced as the final structure in the present study.

4. CONCLUSIONS

In this paper, in order to increase the torque of the axial flux hysteresis motor, different structures were implemented on the hysteresis disc of the motor rotor. These structures include creating a reluctance gap on the hysteresis disc, using magnet parts in the gaps created on the hysteresis disc and using magnet rings in the inner and outer diameters of the hysteresis disc. In order to compare the structures, the attempt was to present these structures in the same dimensions of the initial motor, with a simple structure. Moreover, in order to maintain the starting torque of the hysteresis motor, the volume of the hysteresis material in all structures was considered more significant compared to that of the magnet. The magnetic ring of the hysteresis motor was modeled using elliptical method. Finally, the torque results of different structures were calculated and subsequently analyzed by finite element analysis method. As the results showed, the motor structures with ring magnet combination had more favorable torque. Among the ring magnet combinations, the structure with internal ring magnet had the highest torque.

5. ACKNOWLEDGMENT

We would like to acknowledge the study participants who generously shared their time and insights.

REFERENCES

[1] Md Azizur Rahman and Ruifeng Qin, "Starting and Synchronization of Permanent Magnet Hysteresis Motors," IEEE Trans. Industry Applications, vol.32, no.5, pp.1183-1189, Sept-Oct. 1996.

[2] Bo Gao, Yuan Cheng, Tianxu Zhao, Haodong Sun and Shumei Cui, "A Review on Analysis Methods and Research Status of Hysteresis Motor," *Energies*, vol.16, no.15, pp.5715, July. 2023.

[3] Md Azizur Rahman and Ruifeng Qin, "A Permanent Magnet Hysteresis Hybrid Synchronous Motor for Electric Vehicles," *IEEE Trans. Industrial Electronics*, vol.44, no.1, pp.46-53, Feb. 1997.

[4] Mariusz Jagiela, Tomasz Garbiec and Marcin Kowol, "Design of High-Speed Hybrid Hysteresis Motor Rotor Using Finite Element Model and Decision Process," *IEEE Trans. Magnetics*, vol.50, no.2, pp.861-864, Feb. 2014.

[5] Mehmet Gedikpinar and Omur Aydogmus, "Design of a Self-Starting Hybrid Permanent Magnet Hysteresis Synchronous Motor Connected Directly to the Grid," *Turkish Journal of Electrical Engineering & Computer Sciences*, vol.25, no.3, pp.1657-1668, Jan. 2017.

[6] Md Azizur Rahman, Ali M. Osheiba, "Steady-State Performance of Polyphase Hysteresis-Reluctance Motors," IEEE Transactions on Energy Conversion, vol.EC-1, no.3, pp.129-133, 1986.

[7] Genjiro Wakui, "Hysteresis motor with reaction torque and its analysis," The transactions of the Institute of Electrical Engineers of Japan. B 98, no.9, pp.781-788, 1978.

[8] Sheikh Fazle Rabbi and Md Azizur Rahman, "Equivalent Circuit Modeling of an Interior Permanent Magnet Hysteresis Motor," *in IEEE 27th Canadian Conference on Electrical and Computer Engineering (CCECE)*, Toronto, Canada, May 2014.

[9] Sheikh Fazle Rabbi and Md Azizur Rahman, "Equivalent Circuit Modeling of a Hysteresis Interior Permanent Magnet Motor for Electric Submersible Pumps," *IEEE Trans. Magnetics*, Vol.52, no.7, pp.1-4 Feb. 2016.

[10] Hamid Lesani, Ahmad Darabi, Zahra Nasiri Gheidari and Farid Tootoonchian, "Very Fast Field-Oriented Control for Permanent Magnet Hysteresis Synchronous Motor," *Iranian Journal of Electrical & Electronic Engineering*, vol.2, no.1, pp.34-40, Jan. 2006.

[11] Renato Galluzzi, Nicola Amati and Andrea Tonoli, "Modeling, Design, and Validation of Magnetic Hysteresis Motors," in *IEEE Trans. Industrial Electronics*, vol.67, no.2, pp.1171-1179, Feb. 2020.

[12] Bo Gao, Yuan Cheng, Hoadong Sun and Shumei Cui, "Equivalent Circuit Model of Hysteresis Motor Considering Magnetic Field Harmonics," *2023 IEEE 6th Student Conference on Electric Machines and Systems (SCEMS)*, HuZhou, China, December 2023.

[13] Liang, Cao and Ge Li, "Complete parallelogram hysteresis model for electric machines," *IEEE Trans. Energy Conversion*, vol.25, no.3, pp.626-632, Sept. 2010.

[14] Jack Gieras, R. J. Wang, M. J. Kamper, *Axial Flux Permanent Magnet Brushless Machines*, Springer Science & Business Media, 2008, p.1-17.

[15] Fabio Giulii Capponi, Giulio De Donato, Federico Caricchi, "Recent advances in axial-flux permanent-magnet machine technology," *IEEE Trans. Industry Application*, vol.48, no.6, pp.2190–2205, Nov. 2012.

[16] Amin Mahmoudi, Solmaz Kahourzade, Nasrudin Abd Rahim, Wooi Ping Hew and Mohammad Nasir Uddin, "Design, Analysis, and Prototyping of a Novel-Structured Solid-Rotor-Ringed Line- Start Axial-Flux Permanent-Magnet Motor," *IEEE Trans. Industrial Electronics*, vol.61, no.4, pp.1722-1734, Apr. 2014.

[17] Ali Behniafar, Ahmad Darabi, "A New Semianalytical Method for Analysis of the Disc-Type Permanent Magnet Hysteresis Motor in Steady-State Operational Conditions," *Turkish Journal of Electrical Engineering & Computer Sciences*, vol.26, no.1, pp.542-553, Jan. 2018.

[18] Ali Behniafar, Ahmad Darabi, "Analytical Modeling of Disc-Type Permanent Magnet Hysteresis Motor in Steady-State Operational Conditions," *COMPEL-The international journal for computation and mathematics in electrical and electronic engineering*, vol.36, no.4, pp.991-1007, July. 2017

[19] Reza Nasiri-Zarandi, Mojtaba Mirsalim and Alberto Tenconi, "A Novel Hybrid Hysteresis Motor with Combined Radial and Axial Flux Rotors," *IEEE Trans. Industrial Electronics*, vol.63, no.3, pp.1684-1693, March. 2016.

[20] Ali Akbar Nasiri and Mojtaba Mirsalim, "Analysis of a Reverse Hybrid Hysteresis Motor Using Hyperbolic Modelling of Hysteresis Loop," *IET power Applications*, vol.14, no.8, p.1339-1346, Aug. 2020.

[21] M. L. Hodgdon, "Applications of a Theory of Ferromagnetic Hysteresis," *IEEE Trans. Magnetics*, vol.24, no.1, pp.218-221, Jan. 1988.

[22] David C. Jiles and David L. Atherton, "Theory of Ferromagnetic Hysteresis," *Journal of Magnetism and Magnetic Materials*, vol.61, no.2, pp.48-60, Nov. 1986.

[23] Ajay P. S. Baghel and Shrikrishna V. Kulkarni, "Dynamic Loss Inclusion in the Jiles–Atherton (JA) Hysteresis Model Using the Original JA Approach and the Field Separation Approach," *IEEE Trans. Magnetics*, vol. 50, no. 2, pp. 369-372, Feb. 2014.

[24] Isaak D. Mayergoyz, "Mathematical models of hysteresis," Magnetics, *IEEE Trans. Magnetics*, vol.22, no.5, pp.603-608, Sep.1986.
[25] Shaolin Li, Qiwei Xu and Qian Wang, "Researchon Global Temperature Rise Characteristics of Hysteresis Motor Based on Dynamic Loss Model," *in The Proceedings of the 17th Annual Conference of China Electrotechnical Society* Singapore, April 2023.
[26] Farouk A.A.Zaher, "An Analytical Solution for the Field of a Hysteresis Motor Based on Complex Permeability," *IEEE Trans. Energy Conversion*, vol.5, no.1, pp.156-163, March. 1990.
[27] Reza Nasiri-Zarandi, and Mojtaba Mirsalim, "Analysis and Torque Calculation of an Axial Flux Hysteresis Motor Based on Hyperbolic Model of Hysteresis Loop in Cartesian Coordinates," *IEEE Trans. Magn*etics, vol.51, no.7, pp.1-10, July. 2015.
[28] Reza Nasiri-Zarandi, Mojtaba Mirsalim, "Finite-Element Analysis of an Axial Flux Hysteresis Motor Based on Complex Permeability Concept Considering the Saturation of the Hysteresis Loop," *IEEE Trans. Industry Applications*, vol.52, no.2, pp.1390-1397, Oct. 2016.
[29] Maxime Tousignant, Frederic Sirois, Gerard Meunier and Christophe Guerin, "Incorporation of a Vector Preisach–Mayergoyz Hysteresis Model in 3-D Finite Element Analysis," *IEEE Trans. Magnetics*, vol.55, no.6, pp.1-4, June. 2019.
[30] Hamidreza Mizani, Ahmad Darabi and Siamak Omrani, "A New Hybrid Hysteresis Reluctance Disc Type Motor; design, Prototyping and Analysis," *International Conference of Electrical and Electronic Technologies for Automotive*, Milan, Italy, July 2018.
[31] Teymoor Ghanbari, Mohsen Sanati Moghadam, Ahmad Darabi, "Comparison Between Coreless and Slotless Kinds of Dual Rotor Discs Hysteresis Motors," *IET Electric Power Application*, vol.1, no.10, pp.133–140, Feb. 2016.
[32] Alejandro Rojas, Juan A. Tapia and M. Anibal Valenzuela, "Axial flux PM Machine Design with Optimum Magnet Shape for Constant Power Region Capability," *18th International Conference on Electrical Machines*, Vilamoura, Portugal, September 2008.
[33] Jack Gieras, *Permanent Magnet Motor Technology: Design and Applications*, CRC Press, 2010, p119-173.
[34] Saeid Javadi and Mojtaba Mirsalim, "A Coreless Axial-Flux Permanent-Magnet Generator for Automotive Applications," *IEEE Trans. Magnetics*, vol.44, no.12, pp.4591-4598, Dec. 2008.
[35] Edouard Bomme, Albert Foggia and Thierry Chevalier, "Double Air-Gaps Permanent Magnets Synchronous Motors Analysis," *18th International Conference on Electrical Machines*, Vilamoura, Portugal, September 2008.
[36] Wenjie Cheng, Wei Li, Ling Xiao, Ming Li, Bin Zhong and Hongwei Fan, "Rotor Design of Ultra-high Speed PM Motor with Self-starting Ability," *IEEE International Conference on Mechatronics and Automation (ICMA)*, Changchun, China, October 2018.
[37] Ali Behniafar and Ahmad Darabi, "A New Design Algorithm for the PMHS Motor Considering the Combination Ratio," *Turkish Journal of Electrical Engineering and Computer Sciences*, vol.29, no.3, pp.1582–1597 Jan. 2021.